SUPPLEMENTARY DATA

Modular Maturation and Novel Assembly Factors in the Biogenesis of Human Mitochondrial Small Ribosomal Subunit

Supplementary Figure 1

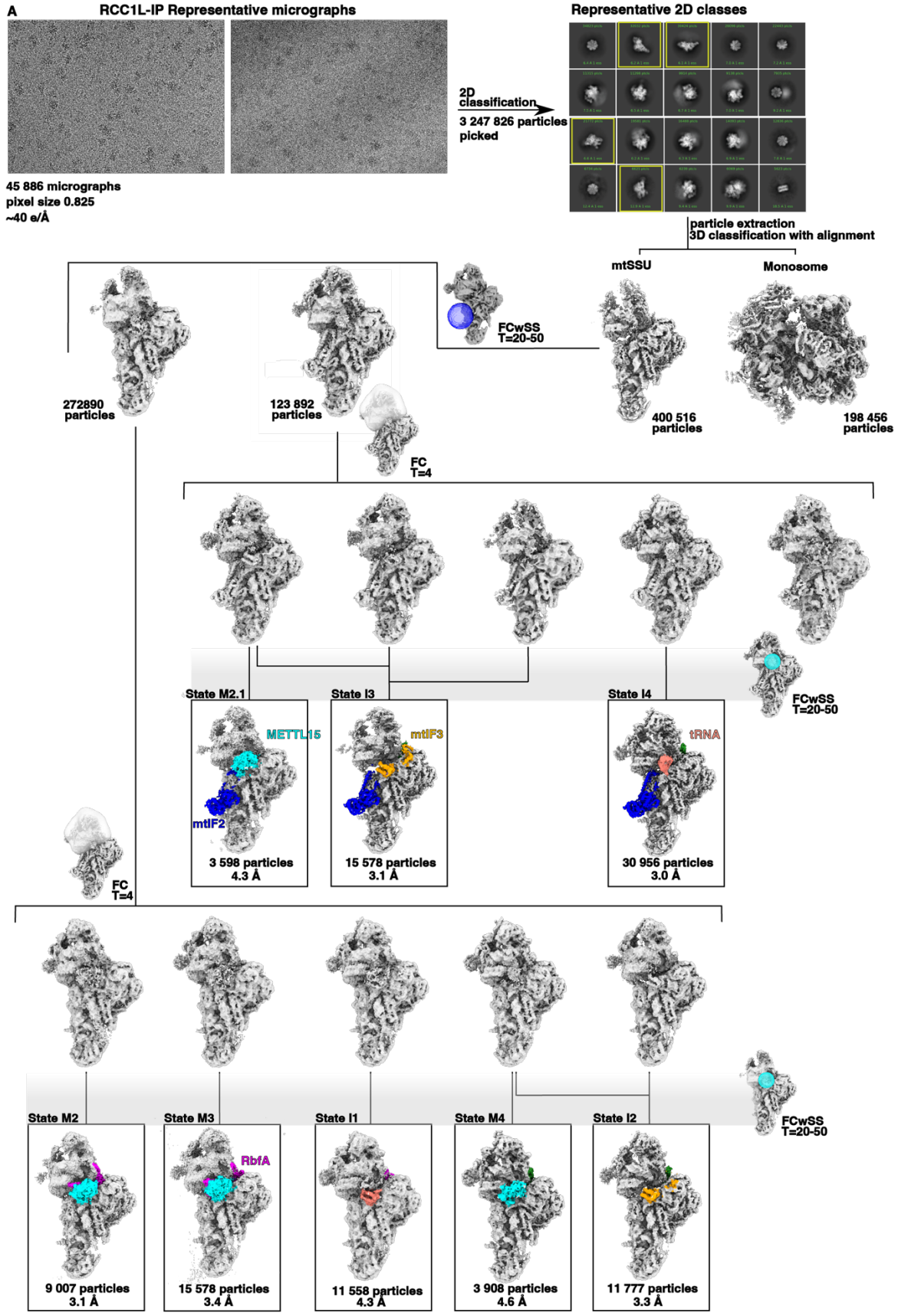

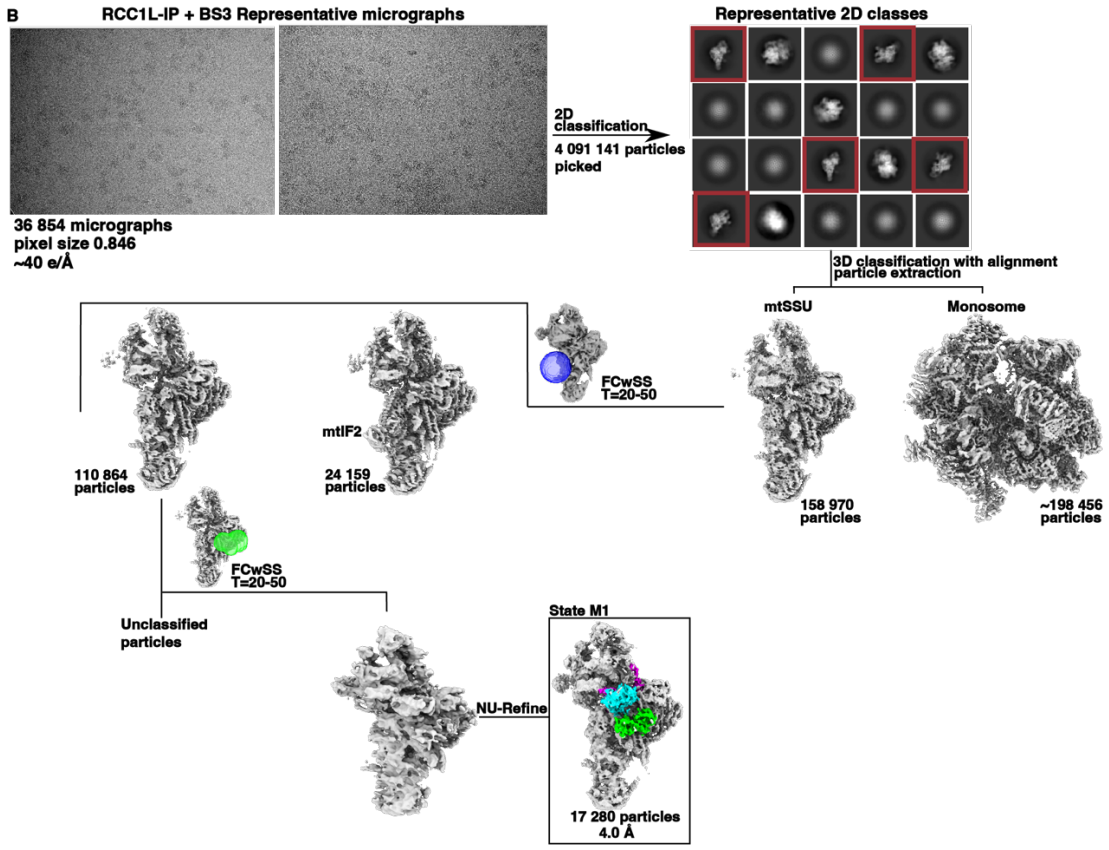
B
RCC1L-IP + BS3 Representative micrographs
36 854 micrographs
pixel size 0.846
~40 e/Å
2D classification
4 091 141 particles picked
Representative 2D classes
3D classification with alignment particle extraction
mtSSU
Monosome
158 970 particles
~198 456 particles
FCwSS T=20-50
110 864 particles
mtIF2
24 159 particles
FCwSS T=20-50
Unclassified particles
NU-Refine
State M1
17 280 particles
4.0 Å

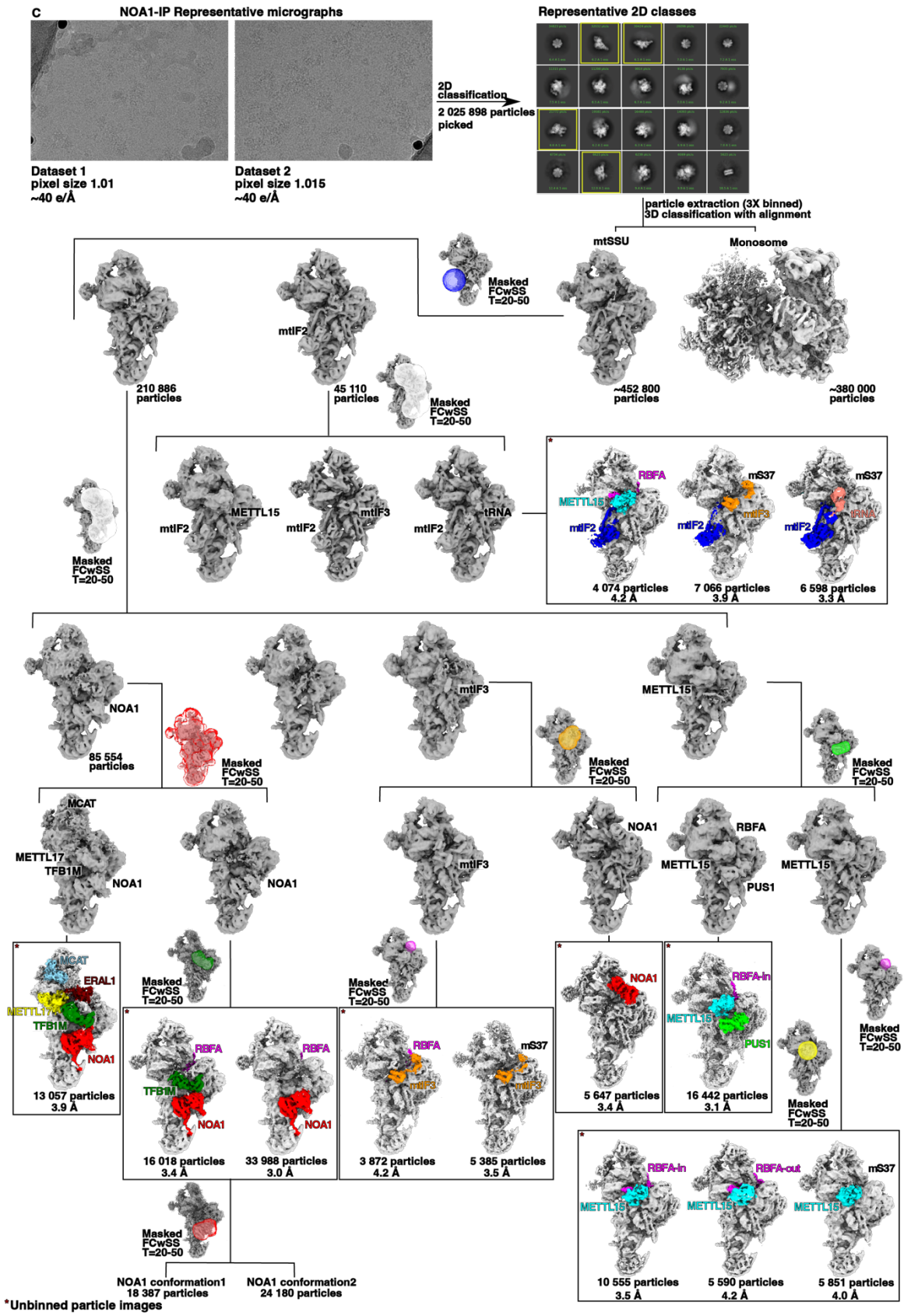
C
NOA1-IP Representative micrographs
Dataset 1
pixel size 1.01
~40 e/Å
Dataset 2
pixel size 1.015
~40 e/Å
2D classification
2 025 898 particles picked
Representative 2D classes
particle extraction (3X binned)
3D classification with alignment
mtSSU
Monosome
Masked FCwSS T=20-50
210 886 particles
mtIF2
45 110 particles
~452 800 particles
~380 000 particles
METTL15
mtIF3
tRNA
RBFA
mS37
4 074 particles 4.2 Å
7 066 particles 3.9 Å
6 598 particles 3.3 Å
NOA1
85 554 particles
MCAT
METTL17
TFB1M
ERAL1
13 057 particles 3.9 Å
16 018 particles 3.4 Å
33 988 particles 3.0 Å
3 872 particles 4.2 Å
5 385 particles 3.5 Å
PUS1
RBFA-in
5 647 particles 3.4 Å
16 442 particles 3.1 Å
RBFA-out
10 555 particles 3.5 Å
5 590 particles 4.2 Å
5 851 particles 4.0 Å
NOA1 conformation1
18 387 particles
NOA1 conformation2
24 180 particles
*Unbinned particle images

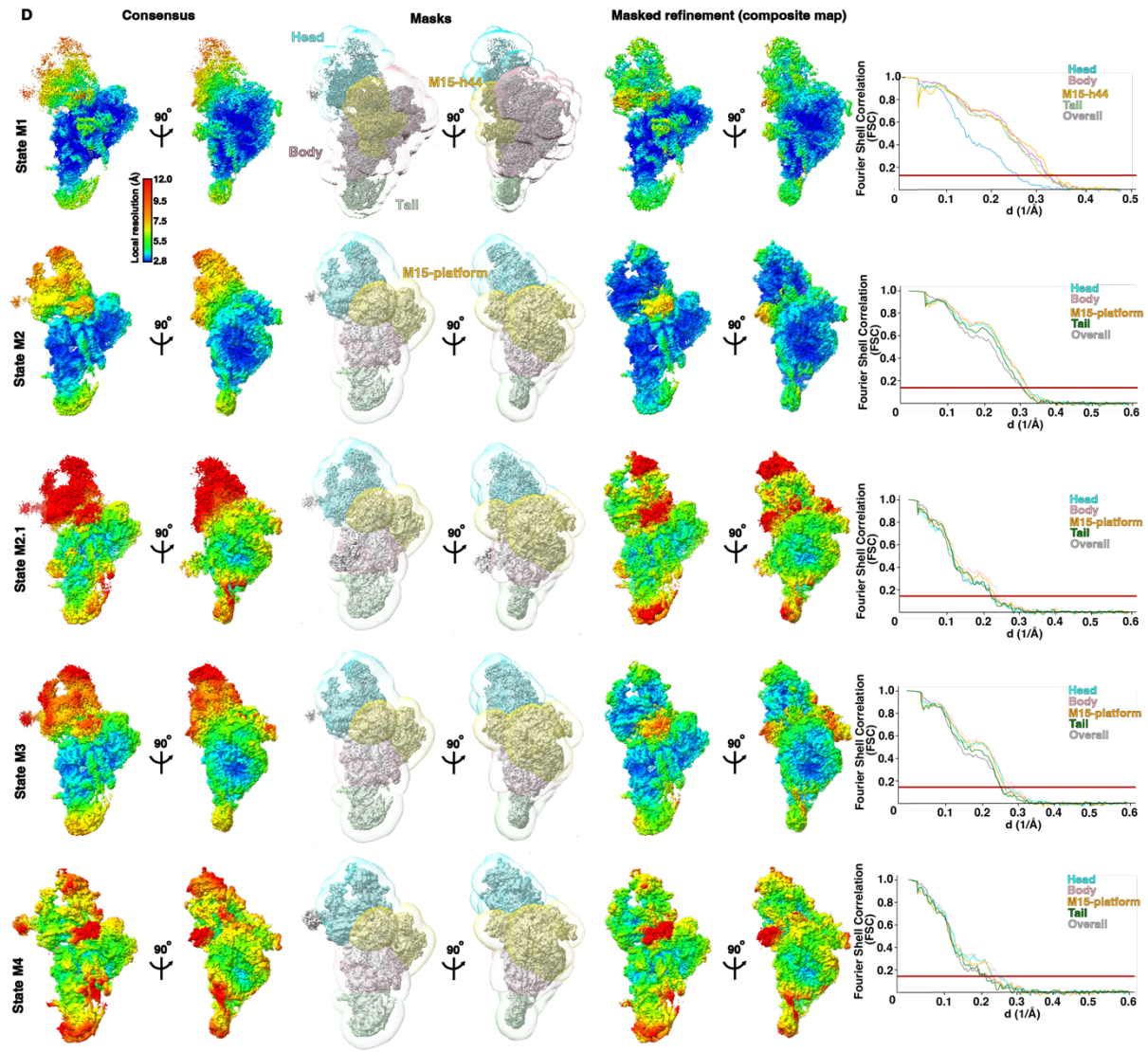
D
Consensus
Masks
Masked refinement (composite map)
State M1
State M2
State M2.1
State M3
State M4
90°
Local resolution (Å)
12.0
9.5
7.5
5.5
2.8
Head
Body
Tail
M15-h44
M15-platform
Fourier Shell Correlation (FSC)
d (1/Å)
Head
Body
M15-h44
Tail
Overall
Head
Body
M15-platform
Tail
Overall

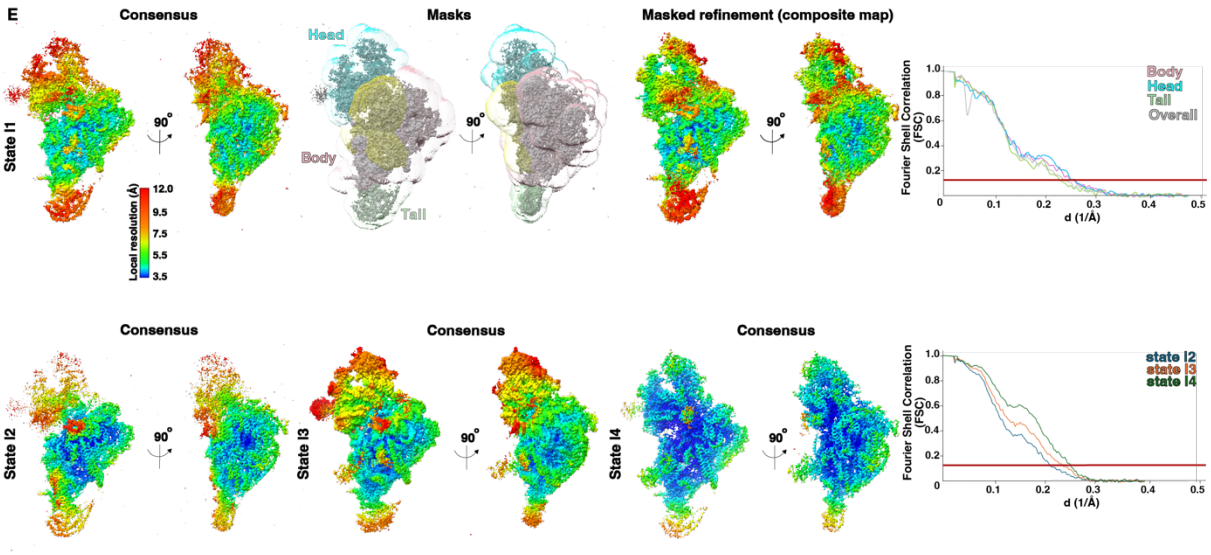
E
Consensus
Masks
Masked refinement (composite map)
State I1
State I2
State I3
State I4
90°
Local resolution (Å)
12.0
9.5
7.5
5.5
3.5
Head
Body
Tail
Fourier Shell Correlation (FSC)
d (1/Å)
Body
Head
Tail
Overall
state I2
state I3
state I4

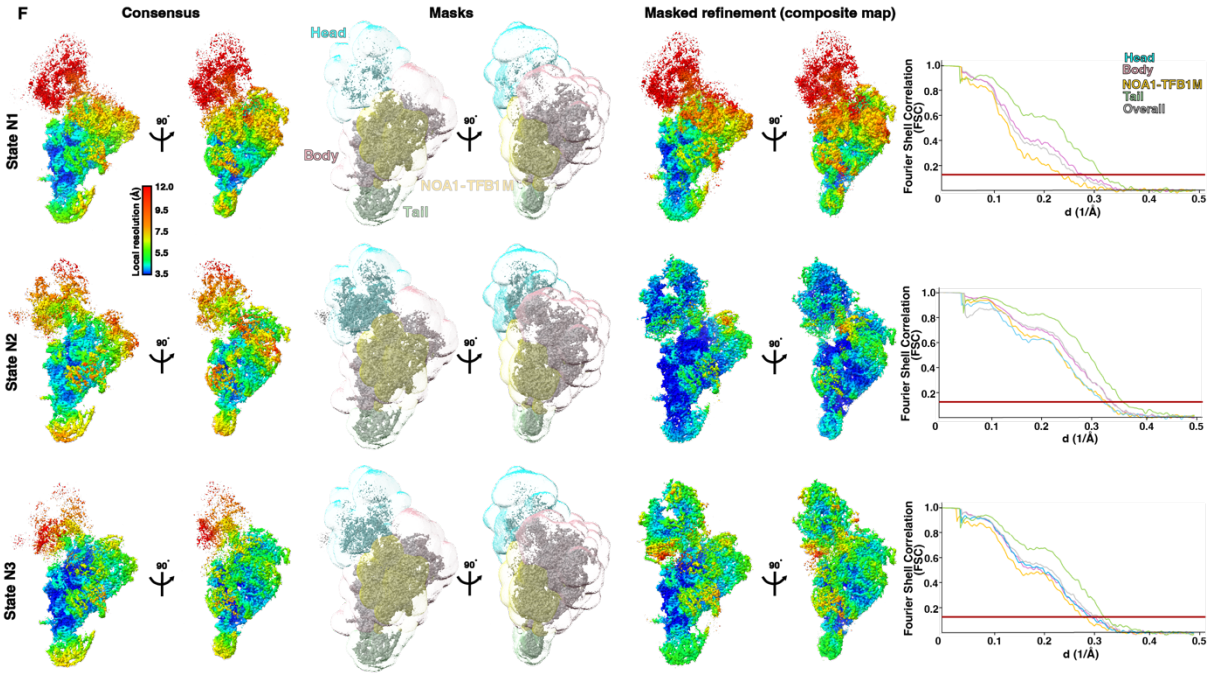

Supplementary Figure 1. Cryo-EM data processing.

(A-C) The overview of the cryo-EM data processing scheme highlighting the 3D classification strategy employed to identify mtSSU assembly intermediates from RCC1L-IP datasets **(A,B)** and NOA1-IP datasets **(C)**. **(D-F)** Local resolution maps of consensus reconstructions and of the composite maps obtained by merging masked-refined maps from the mtSSU assembly states clustered as METTL15-containing **(D)**, initiation-factor(s)-containing classes **(E) and** NOA1-containing **(F)**. Masking scheme is shown in the central panels. Corresponding FSC curves are shown where the red line marks FSC=0.143.

Supplementary Figure 2

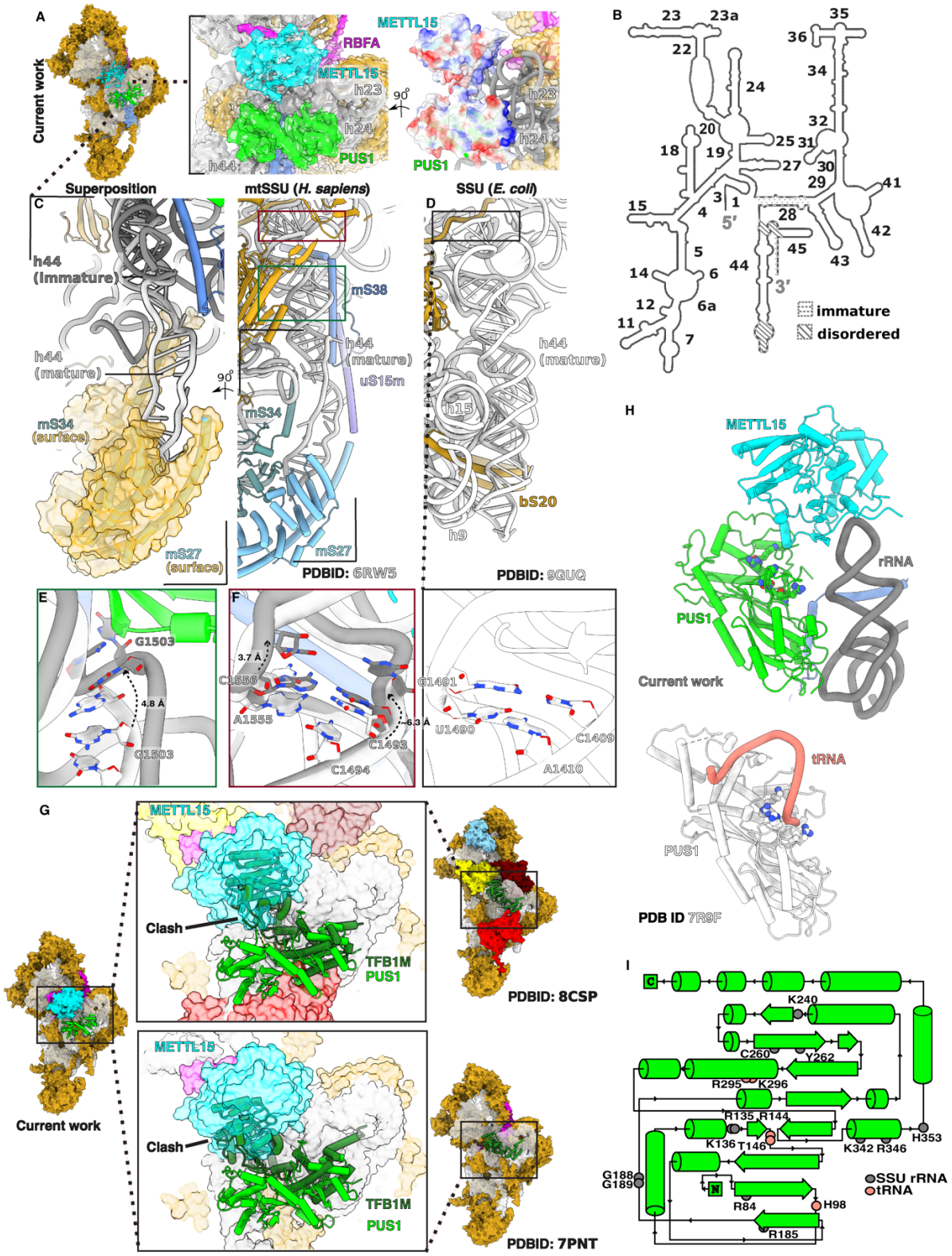

Supplementary Figure 2. Structural features of METTL15-PUS1 bound assembly intermediate.

(A) METTL15-PUS1-RBFA bound to SSU assembly intermediate together with density (colored by zone). Electrostatic potential surface of METTL15 and PUS1 form the interface with rRNA. **(B)** 2D representation of 12S rRNA in this assembly state with indicated disordered regions (solid lines). **(C)** Superposition (left panel) between PUS1-h44 (current work) and mature h44 (right panel) docked inside mS27 cleft (yellow surface)**. (D)** Mature h44 in *E.coli* SSU (PDBID 9GUQ). Zoom-in panel shows base-pairs close to the decoding center (white). **(E,F)** PUS1-induced conformational change in h44: **(E)** flipping-out of G1503 (dark grey) in comparison with mature h44 (light grey, transparent cartoon) is indicated; **(F)** non base-pairing residues kinked in immature h44 (current work). **(G)** Superposition between PUS1 (light green, cartoon) and TFB1M (dark green, cartoon) in its two reported conformations (PDBID 8CSP[6] and 7PNT[7]). All other mtSSU components are shown in surface. METTL15 is shown in transparent surface to highlight the clash with TFB1M. **(H)** Comparison of the human PUS1-rRNA complex from the current work (top) with PUS1-RNA complex from *S. cereviseae* (PDB 7R9F, bottom). **(I)** Topology diagram of human PUS1 marks the residues interacting with rRNA (grey) and those implicated in pseudouridylation activity (salmon).

Supplementary Figure 3

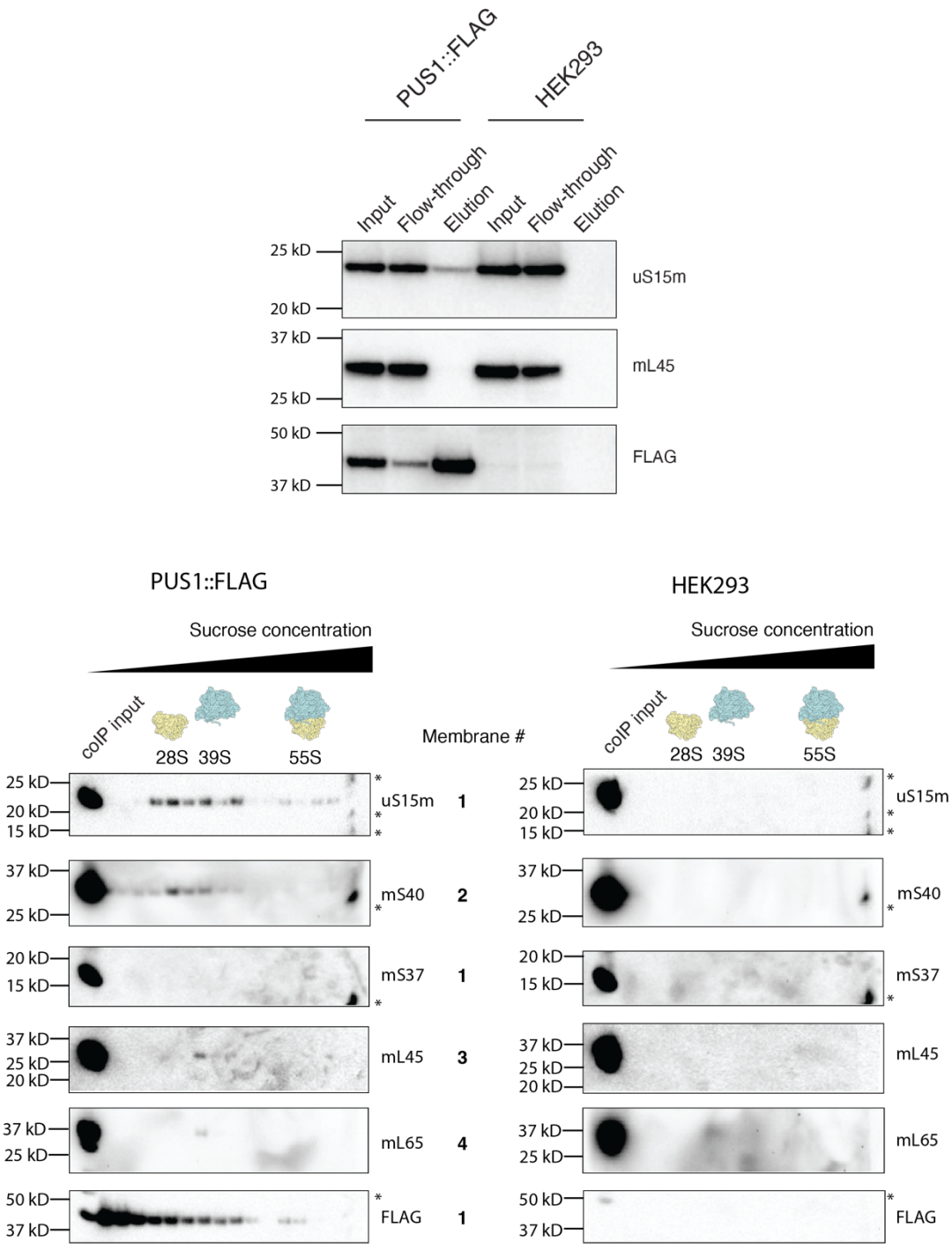

Supplementary Figure 3. Characterization of PUS1-mtSSU interactions.
Co-IP elution of PUS1::FLAG (Western blotting at the top panel) was resolved by a sucrose gradient centrifugation and probed for mitoribosome components (bottom left panel). Elution from HEK293 was used as a negative control (top and bottom right panels). Asterisk (*) indicates non-specific bands. "Membrane #" indicates the number of the membrane used for the probing. All the membranes were obtained from the sample of the same co-IP experiment. "coIP input" lane corresponds to the "Input" sample from the coIP experiment; its signal was adjusted to mask the oversaturated pixels.

Supplementary Figure 4

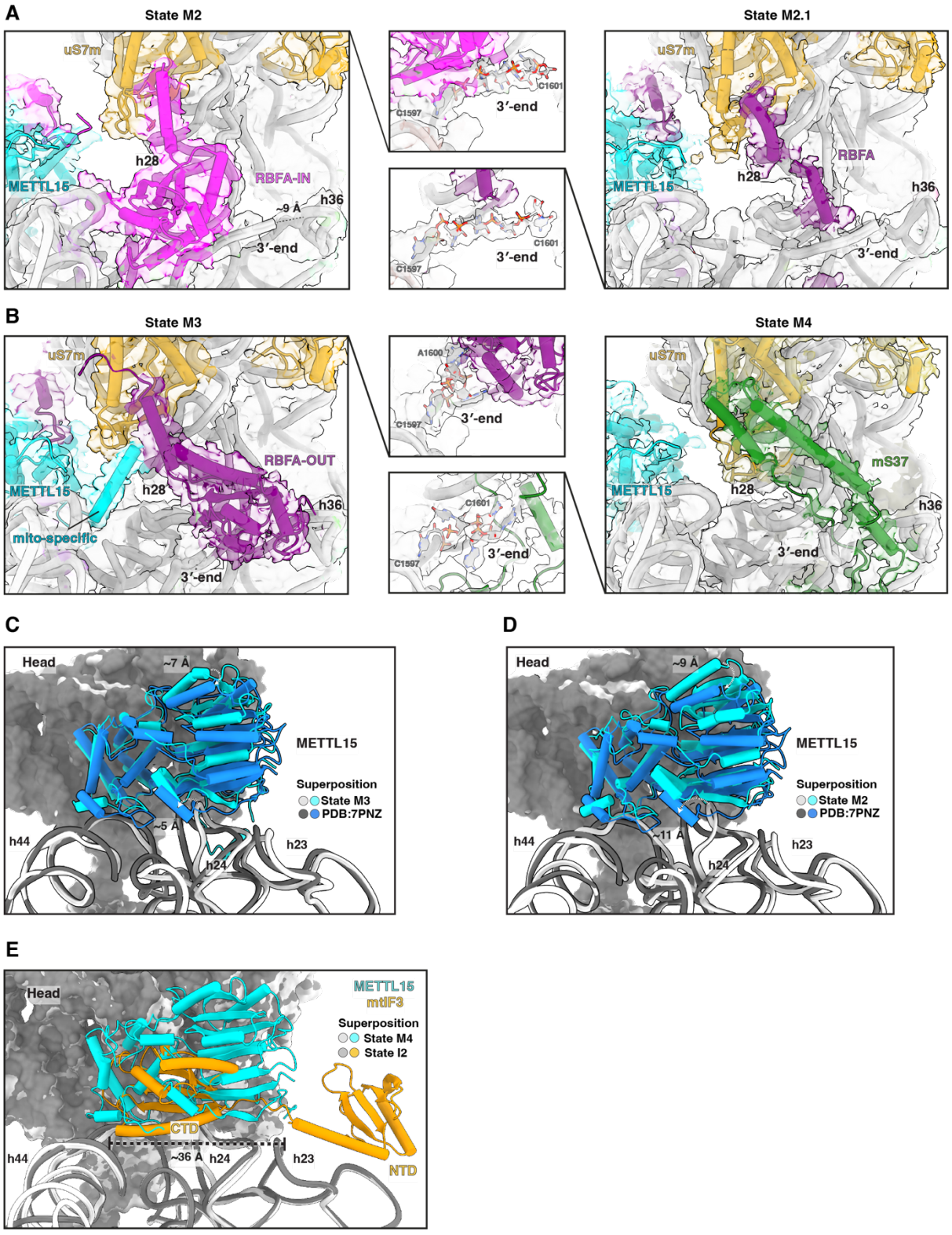

Supplementary Figure 4. 3′-end rRNA maturation and re-positioning of the platform in METTL15-bound assembly intermediates.

(A) The panels (left and right) illustrate the overall immature folding of 3′-end rRNA in states M2 and M2.1 with RBFA (magenta and purple), uS7m (gold) and METTL15 (cyan), shown with the density map. The state M2.1 signifies RBFA in transition between IN and OUT (purple) conformation. The 3′-end rRNA makes contact with the RBFA and assumes similar fold in both assembly states. The zoom-in panels show the density for the 3′-end nucleotides (nt. 1597-1600) stabilized by contacts with the RBFA, in both the states.
(B) The panels (left and right) illustrate the folding of 3′-end rRNA in states M3 and M4. In state M4, mS37 (green) substitutes RBFA. The OUT conformation of RBFA allows 3′-end rRNA to be placed between the head and the platform, where the final folding is guided by mS37. The zoom-in panels show the density of the 3′-end nucleotides (nt. 1597-1601). The 3′-end rRNA interacts with mS37 and adopts its final conformation.
(C-D) Superposition of the final METTL15-RBFA-OUT state (PDB:7PNZ) with state M3 (left) and M2 (right), reveals the overall movement of METLL15 on mtSSU correlating with the shift in the platform (h23-h24). The color code for each state is indicated in the panel alongside.
(E) Superposition of METTL15 and mtIF3 from states M4 and I2 shows that METTL15 and mtIF3-CTD occupy similar space on h24 and 44, spanning a distance of ~36 Å. The binding contributes to the stabilization of the platform and blocks the decoding region prior to the recruitment of P-tRNA. The color code for each state is indicated in the panel alongside.

Supplementary Figure 5

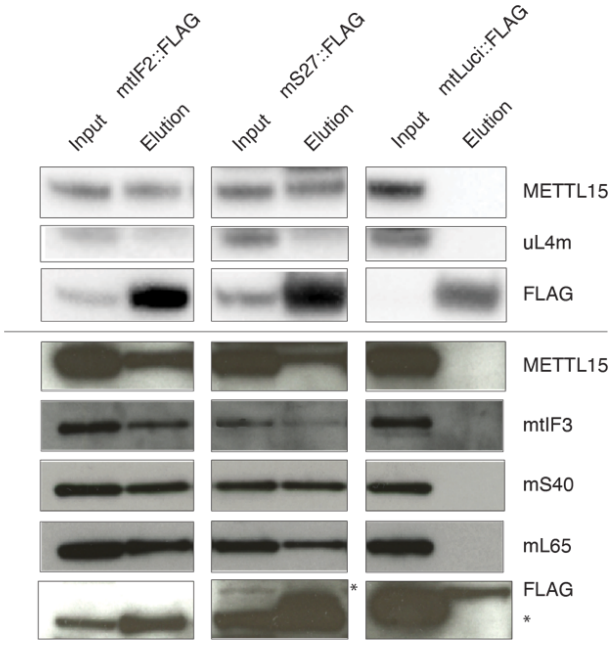

Supplementary Figure 5. Characterization of METTL15-mtIF2 interaction.

Western blot analysis of FLAG immunoprecipitation experiments (IP) using mtIF2::FLAG as bait. IP experiments with FLAG-tagged mS27 (mtSSU protein) and mitochondrially targeted luciferase (mtLuci) were used as controls. METTL15 co-precipitates with the overexpressed mtIF2::FLAG and mS27 but not mtLuci. Grey horizontal line separates the results of two independent experiments.

Supplementary Figure 6

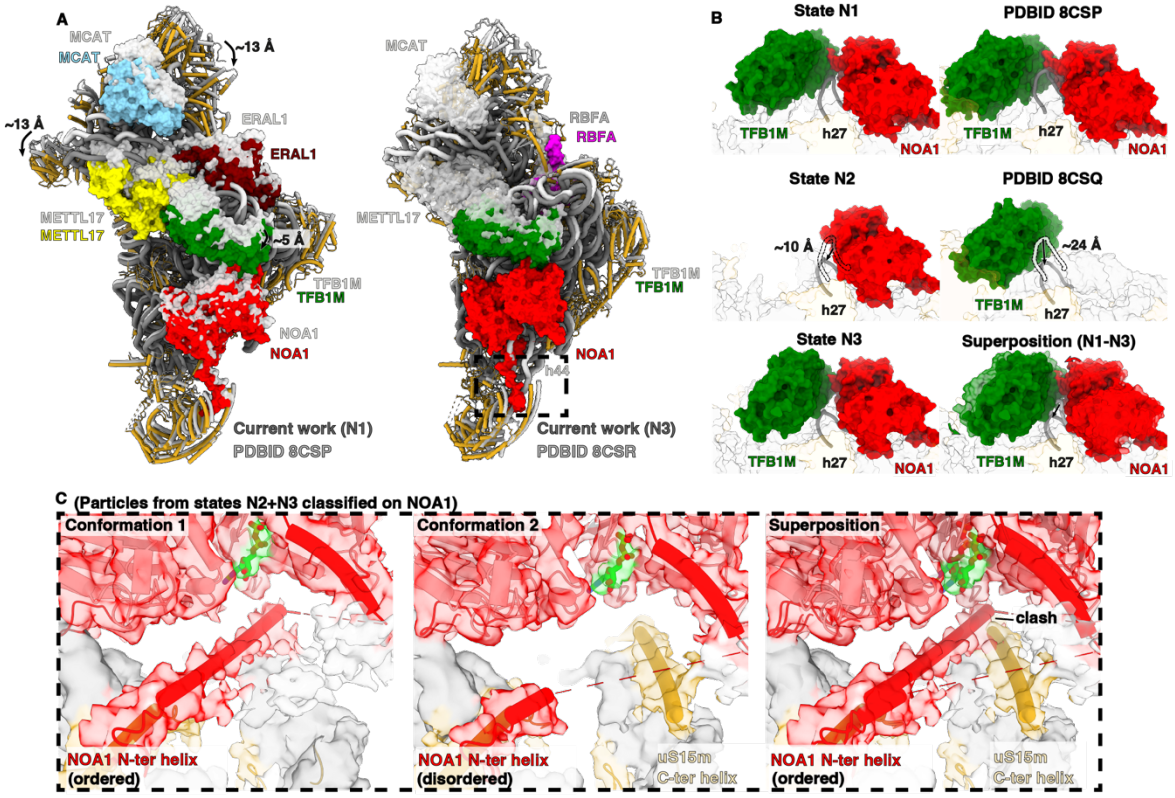

Supplementary Figure 6. Structural comparison of NOA1-bound assembly intermediates from current and previous works.

(A) Left: superposed models of state N1 (colored) and PDB 8CSP (white) show relative movement. Bound assembly factors are shown as surface. Right: superposed models of state N3 (colored) and PDB 8CSR[6] (white) highlight differences in head and body maturation.
(B) Maturation of h27 in states N1-N2 (left) versus published work[6] (right). and in state A3 (lower panel, left) together with superposition between states A1 and A3 to show the initial and final conformations of NOA1, TFB1M, and h27 (lower panel, right). Conformational changes are indicated in arrows.
(C) The zoom-in panel shows the density for the N-terminal mito-specific helix of NOA1 (states N2-N3) resolved into ordered (left) and partly disordered (center) conformations. This allows structuring of the C-terminal helix of uS15m (center). Superposition (right) reveals a steric clash between the two elements. Density is shown as a colored surface.

Supplementary Figure 7

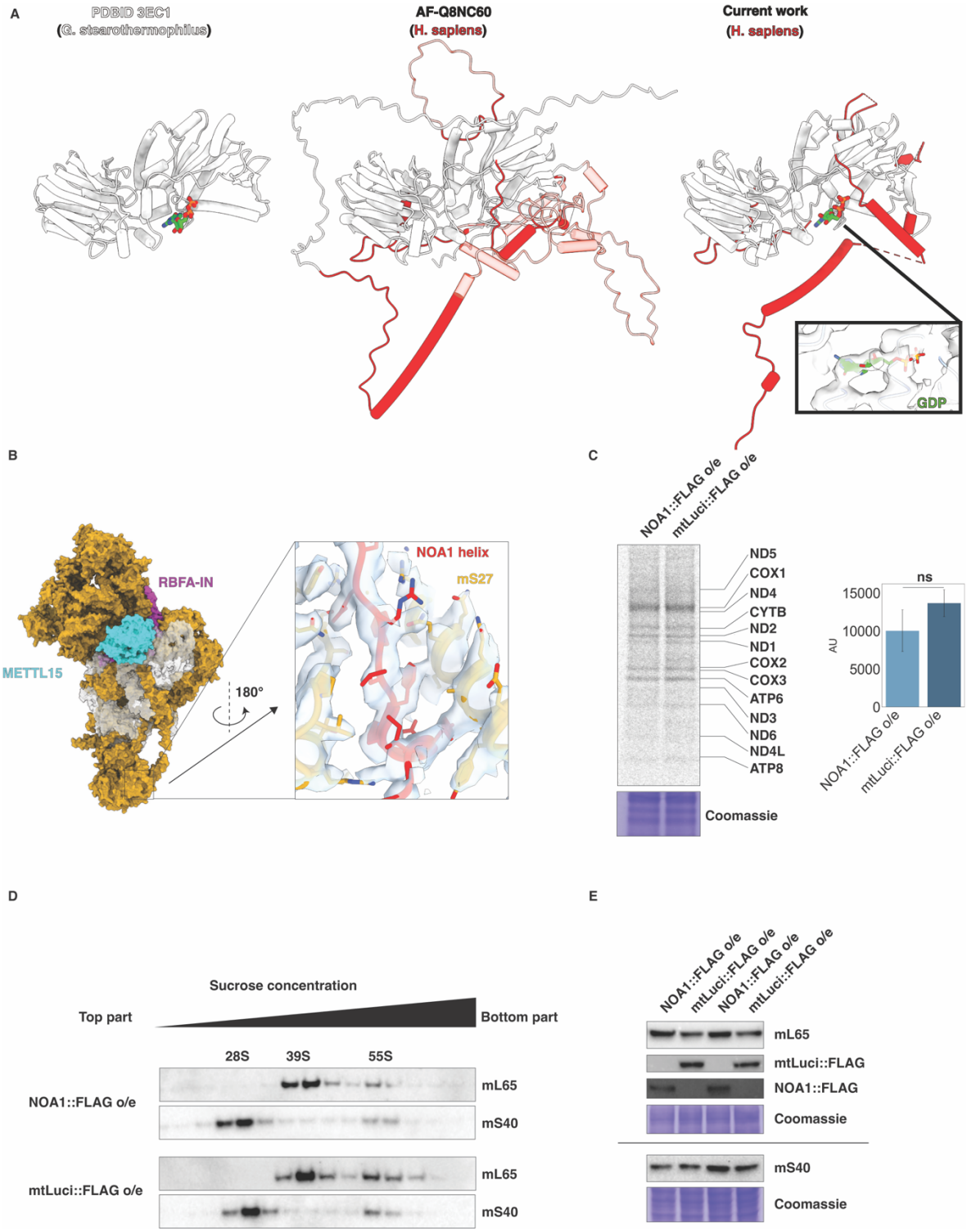

Supplementary Figure 7. NOA1::FLAG overexpression does not cause major disruptions in mitochondrial translation.

(A) Structural comparison of NOA1 from current and published work. Structure of NOA1 from *G. stearothermophilus* (PDB 3EC1, left), alphafold model of human NOA1 (AF-Q8NC60) and in current work. Mito-specific elements are colored red, and unmodeled regions are transparent. **(B)** METTL15-IN state (left) shown as the representative model to illustrate the N-terminal loop of NOA1 bound to mS27 in mtSSU tail together with the density (zoom-in). This feature is common to all 'NOA1' models reported in this work.
(**C**) Left panel: autoradiography of *de novo* labeling of mitochondrial translation with 35S-labeled methionine and cystine. FLAG-tagged mitochondrially targeted luciferase overexpression (mtLuci::FLAG o/e) was used as a control. Right panel: quantification of band intensities. The data represent mean +/-1 standard deviation from three independent experiments.
(**D**) Sucrose gradient centrifugation analysis to assess mitoribosome sedimentation patterns in cells overexpressing NOA1::FLAG compared to mtLuciferase. Mitochondrial lysates were loaded onto 10-30 % isokinetic sucrose gradients and obtained fractions were analyzed via western blotting. Membranes were probed for mtLSU: MRP mL65 and mtSSU: MRP uS40m.
(**E**) Western blotting to assess steady-state levels of MRPs (mL65 and MRP uS40m) in cells overexpressing FLAG-tagged NOA1 or mtLuciferase. Loading was determined using Coomassie staining (n = 3 independent experiments).

Supplementary Table 1. Cryo-EM data collection, processing and model refinement statistics

Data collection and processing	**state N1**	**state N2**	**state N3**	**state M1**	**state M2**	**state M2.1**	**state M3**	**State M4**	**state I1**	**state I2**	**state I3**	**state I4**
Microscope	Titan Krios	Titan Krios	Titan Krios	Titan Krios	Titan Krios	Titan Krios	Titan Krios	Titan Krios	Titan Krios	Titan Krios	Titan Krios	Titan Krios
Detector	K3	K3	K3	K3	K3	K3	K3	K3	K3	K3	K3	K3
Magnification	165,000	165,000	165,000	165,000	165,000	165,000	165,000	165,000	165,000	165,000	165,000	165,000
Voltage [kV]	300	300	300	300	300	300	300	300	300	300	300	300
Total electron exposure [e^{-}/Å^2]	42-45	42-45	42-45	42-45	42-45	42-45	42-45	42-45	42-45	42-45	42-45	42-45
Defocus range [μm]	-0.3 to -1.9	-0.3 to -1.9	-0.3 to -1.9	-0.3 to -1.9	-0.3 to -1.9	-0.3 to -1.9	-0.3 to -1.9	-0.3 to -1.9	-0.3 to -1.9	-0.3 to -1.9	-0.3 to -1.9	-0.3 to -1.9
Exposure rate (e−/Å^2/sec)	20 to 25	20 to 25	20 to 25	20 to 25	20 to 25	20 to 25	20 to 25	20 to 25	20 to 25	20 to 25	20 to 25	20 to 25
Number of frames	40-42	40-42	40-42	40-42	40-42	40-42	40-42	40-42	40-42	40-42	40-42	40-42
Pixel size [Å]	0.505	0.505	0.505	0.505	0.825	0.825	0.825	0.825	0.825	0.825	0.825	0.825
Symmetry imposed	C_1	C_1	C_1	C_1	C_1	C_1	C_1	C_1	C_1	C_1	C_1	C_1
Processed particles (no.)	452,800	452,800	452,800	452,800	198,456	198,456	198,456	198,456	198,456	198,456	198,456	198,456
Final particles (no.)	13,057	33,988	16,018	16,442	9,007	3,598	15,578	3,908	3,872	11,558	15,578	30,956
Map resolution [Å] (overall)	3.9	3.03	3.4	3.1	3.9	4.3	3.2	4.6	4.2	4.5	3.2	3.0
FSC threshold	0.143	0.143	0.143	0.143	0.143	0.143	0.143	0.143	0.143	0.143	0.143	0.143
Resolution min/median/max [Å]	3.0/7.5/24.6	3.1/7.3/26.2	2.8/6.2/22.3	2.7/4.6/21.4	3.4/6.8/24.8	3.3/8.2/25.8	3.0/4.9/15.9	3.1/7.7/33.5	3.3/6.9/24.8	4.1/6.0/24.6	3.0/.2/28.3	2.8/4.19.3
Map-sharpening *B*-factor (overall)	-42.2	-29	-29	-23	-37.1	-38.5	-35.3	-36.5	-34.3	-34.7	-31.1	-30.4
Refinement												
Model composition												
Total atoms (non-hydrogen/hydrogen)	1272601/59903	1225564/57421	1296667/60765	1341330/62568	1272933/59156	1330831/62078	1281227/59502	1287522/59812	1277821/59241	-	-	-
Chains (protein/RNA)	32/1	33/1	34/1	39/1	40/1	45/1	42/1	45/1	38/1	-	-	-
RNA residues	749	803	852	926	906	905	923	930	937	-	-	-
Protein residues	6387	5901	6232	6357	5,988	6,370	6,007	6,028	5,949	-	-	-

Metal ions (Mg2+/ K+/Zn2+)	0/0/1	42/11/ 1	41/10/ 1	40/6/1	31/0/1	24/0/1	13/0/1	2/0/1	61/17/ 1	-	-	-
Ligands (2Fe-2S/ATP/ GDP/ NAD/other)	2/1/1/ 0/1	2/1/1/ 0/0	2/1/1/ 0/0	2/1/1/ 1/2	2/1/1/ 1/1	2/1/2/ 1/1	2/1/2/ 1/2	2/1/1/ 1/1	2/1/1/ 1/1	-	-	-
Waters	0	0	0	4	5	9	8	8	0	-	-	-
Model to map CC (CC_{mask}/CC_{box}/CC_{peaks}/CC_{volume})	0.67/0 .69/0. 53/0.6 7	0.76/0 .85/0. 73/0.7 7	0.81/0 .86/0. 76/0.8 1/0.77	0.82/0 .88/0. 80/0.8 3	0.70/0 .76/0. 63/0.7 1	0.70/0 .79/0. 64/0.7 1	0.79/0 .84/0. 76/0.8 0	0.72/0 .79/0. 65/0.7 2	0.71/0 .79/0. 66/0.7 2	-	-	-
Resolution [Å] by model-to-map FSC, threshold 0.50 (masked/unmasked)	5.6/7. 9	3.1/3. 4	3.2/3. 7	3.3/	3.5/4. 4	3.8/6. 9	3.1/3. 6	3.9/6. 7	3.8/6. 8	-	-	-
Average *B*-factor (RNA/protein/metal ion and ligand/water)	245/2 57/33 8/-	157/1 11/10 6/-	146/1 55.9/1 14/-	107/1 40/97/ 95	100/1 49/87/ 103	149/1 95/12 4/160	88/12 2/71/8 7	140/1 86/13 2/167	130/1 39/10 3/--	-	-	-
R.m.s. deviations, bond lengths [Å]/bond angles [°]	0.003/ 0.507	0.003/ 0.457	0.002/ 0.408	0.003/ 0.469	0.002/ 0.438	0.002/ 0.443	0.002/ 0.436	0.002/ 0.432	0.001/ 0.355	-	-	-
Validation										-	-	-
Clash score	4.17	3.31	3.92	2.51	2.69	2.24	2.32	2.07	1.60	-	-	-
Rotamer outliers [%]	0	0	0	0	0	0	0	0	0	-	-	-
Ramachandran plot [%] (favored/ allowed/disallowed)	98.08/ 1.92/0 .00	98.95/ 1.01/0 .03	98.34/ 1.65/0 .02	98.15/ 1.85/0 .00	96.92/ 3.07/0 .02	96.24/ 3.68/0 .08	97.03/ 2.9/0. 07	97.75/ 2.23/0 .02	98.42/ 1.58/0 .00	-	-	-
CaBLAM outliers [%]	0.98	0.7	0.89	0.63	1.13	1.13	1.03	0.82	0.81	-	-	-
C_β outliers [%]	0	0	0	0	0	0	0	0	0	-	-	-
MolProbity score	1.18	1.12	1.18	1.03	1.24	1.25	1.18	1.03	0.91	-	-	-
PDB/EMDB accession code	xxxx/ EMD-xxxxx	xxxx/ EMD-xxxxx	xxxx/ EMD-xxxxx	xxxx/ EMD-xxxxx	xxxx/ EMD-xxxxx	xxxx/ EMD-xxxxx	xxxx/ EMD-xxxxx	xxxx/ EMD-xxxxx	xxxx/ EMD-xxxxx	NA/EMD-xxxxx	NA/EMD-xxxxx	NA/EMD-xxxxx